

IEEE Catalog Number: 07TH8953C

ISBN: 1-4244-1174-2

Library of Congress: 2007923395

CLEO[®] / Pacific Rim 2007

The 7th Pacific Rim Conference on Lasers and Electro-Optics

August 26 - 31, 2007 • COEX, Seoul, Korea

• Welcome Message

• Author Index

• Committees

• Search

• Acknowledgment & Copyright

• Help

• Table of Contents

• Exit

August 27, 2007

August 28, 2007

August 29, 2007

August 30, 2007

August 31, 2007

© 2007 IEEE. Personal use of this material is permitted. However, permission to reprint/republish this material for advertising or promotional purposes or for creating new collective works for resale or redistribution to servers or lists, or to reuse any copyrighted component of this work in other works must be obtained from the IEEE.

WP_034	Waveguide Photodiode Having a Thin Absorption Layer <i>Jeong-Woo Park, Hyun-Sung Ko, Eun-Deok Sim, Yong-Soon Baek, and Kyoung-Ock Kim (ETRI, Korea).....</i>	602
WP_035	High-Power Broad-Band Superluminescent Diode Using Selective Area Growth at 1.5-μm Wavelength <i>Jung Ho Song, Kisoo Kim, Young Ahn Leem, and Gyungock Kim (ETRI, Korea).....</i>	604
WP_036	1.3 μm Band InGaAs MQWs with InGaP Metamorphic Graded Buffer Layer on GaAs Substrate <i>Masakazu Arai and Yasuhiro Kondo (NTT Photonics Labs., Japan).....</i>	606
WP_037	Gain Characteristics of Coulomb-Correlated Quantum Wire <i>Ping Huai, Tetsuo Ogawa, Kenichi Asano (Osaka Univ., Japan), Yuhei Hayamizu, Toshiyuki Ihara, Masahiro Yoshita, and Hidefumi Akiyama (Univ. of Tokyo, Japan).....</i>	608
WP_038	1.3-μm Continuous Wave Lasing of InAs Quantum Dots with GaInNAs Covering Layer on GaAs Substrate Grown by Metal-Organic Chemical Vapor Deposition <i>M. Kushibe, R. Hashimoto, M. Ezaki, N. Managaki, G. Hatakoshi (Toshiba Corp., Japan), M. Nishioka, and Y. Arakawa (IIS and RCAST Univ. of Tokyo, Japan).....</i>	610
WP_039	Spatiotemporal Dynamics of Photonic Quantum Ring Laser <i>D.K. Kim and O'Dae Kwon (POSTECH, Korea).....</i>	612
WP_040	Characterization of Silicon Avalanche Photodetectors Fabricated in Standard CMOS process <i>Hyo-Soon Kang, Myung-Jae Lee, and Woo-Young Choi (Yonsei Univ., Korea).....</i>	614
WP_041	Excessive Power Penalty due to Strong External Reflection on an Isolator Free DFB Laser Diode Transmitter <i>Jong Jin Lee and Hyun Seo Kang (ETRI, Korea).....</i>	616
WP_042	Ultraviolet Photocodetector Based on $\text{Mg}_x\text{Zn}_{1-x}\text{O}$ ($0 \leq x \leq 0.36$) Thin Films Deposited by RF Magnetron Sputtering <i>Hsin-Ying Lee, Ming-Yi Wang (Nat'l Formosa Univ., Taiwan), and Ching-Ting Lee (Nat'l Cheng Kung Univ., China).....</i>	618

Characterization of Silicon Avalanche Photodetectors Fabricated in Standard CMOS process

Hyo-Soon Kang, Myung-Jae Lee and Woo-Young Choi

Department of Electrical and Electronic Engineering, Yonsei University, 134 Shinchon-dong, Seodaemoon-gu, Seoul 120-749, Korea

Author email address: wchoi@yonsei.ac.kr

Abstract: We present and characterize silicon avalanche photodetectors (APDs) fabricated with 0.18 μm standard complementary metal-oxide-semiconductor (CMOS) process. When the bias is above the avalanche breakdown voltage, the device exhibits photodetection frequency response peaking due to resonance caused by appearance of inductive components in avalanche region.

CMOS-compatible photodetectors have been widely investigated for application in short-distant optical access network and optical interconnect due to the possibility of low-cost integrated optical receivers, which have photodetector as well as other necessary electronic circuits [1, 2]. However, standard CMOS process has inherent drawbacks attributed to narrow depletion region between P+ source/drain and n-well region and limits bandwidth-efficiency product [2]. To overcome this, avalanche photodetectors (APDs) are very promising owing to their internal gain. Furthermore, InGaAs/InAlAs APD results shows that avalanche process can enhance the gain-bandwidth product with the help of the internal rf-gain effect in avalanche region [3].

In this work, we present and characterize CMOS-compatible avalanche photodetectors (CMOS-APD) fabricated with 0.18 μm standard CMOS process without any process modification or a special substrate. By adopting the bias above avalanche breakdown voltage, CMOS-APD exhibits rf-peaking in photodetection frequency response as observed in InGaAs/InAlAs APD [3]. We clarify the physical origin of rf-peaking effect by the examination of impedance characteristics.

Fig. 1 shows the cross-sectional diagram of fabricated CMOS-APD. To eliminate slow diffusion currents, only vertical P+/n-well junction is used and multi-finger electrode with narrow finger space of 0.5 μm is formed. The vertical PN-junction structure can also mitigate the edge breakdown in the avalanche regime. The active area of our CMOS-APD is about $30 \times 30 \mu\text{m}^2$ and the salicide process is blocked for the optical window.

For characterization of the device, all experiments were done on wafer and 850 nm laser diode as well as electro-optic modulator are used. Fig.2 shows photocurrent and avalanche gain as well as current-voltage (I-V) characteristics with and without optical illumination. The fabricated CMOS-APD has avalanche breakdown voltage (V_{BK}) of 10.2 V and maximum avalanche gain of about 1250 at V_{BK} under 0.1 mW optical illumination. Fig. 3 shows the photodetection frequency response of CMOS-APD when the incident optical power is 0.2 mW. Interestingly, at reverse bias voltage (V_{R}) larger than V_{BK} , rf-peaking is observed at the high frequency region. Such rf-peaking has been also reported in InGaAs/InAlAs APD [3]. The rf-peaking can be explained by changes in the impedance characteristics of CMOS-APD in avalanche region. As in transit-time diode such as IMPATT diode, the impedance of CMOS-APD can have an inductive component at V_{R} above V_{BK} in avalanche region [4] and this inductive component can cause rf-peaking. Fig. 4 shows measured reflection coefficients of the device from 50 MHz to 13.5 GHz using vector network analyzer with on-wafer calibration. At V_{R} of 10.0 V, CMOS-APD does not have any inductive components. However, at V_{R} larger than V_{BK} , the device reactance changes from capacitive to inductive and then again to capacitive as the frequency increases. From this impedance

characteristic on Smith chart, it is believed that CMOS-APD has inductive component as well as capacitive component in avalanche regime. We can expect that these inductive and capacitive components can cause resonance which results in rf-peaking in photodetection frequency response.

In Fig. 3, it is noted that the rf-peak frequency increases with increasing V_R . This can be explained by the fact that the inductance in avalanche region is inversely proportional to the current [4] and the CMOS-APD current increases as V_R increases as shown in Fig. 2.

In summary, Si APD devices were fabricated in standard CMOS process and characterized. When the bias above avalanche breakdown voltage, CMOS-APD exhibits rf-peaking in photodetection frequency response due to resonance caused by appearance of inductive components in avalanche region. Through the results, it is expected that the optimization of the CMOS-APD utilizing rf-peaking can enhance photodetection 3-dB bandwidth while maintaining sufficient avalanche gain.

References

- [1] D. M. Kuchta *et al.*, *IBM Journal of Research and Development*, vol. 39, p. 63, 1995.
- [2] T. K. Woodward *et al.*, *Selected Topics in Quantum Electronics, IEEE Journal of*, vol. 5, pp. 146-156, 1999.
- [3] G. Kim *et al.*, *Applied Physics Letters*, vol. 83, pp. 1249-1251, 2003.
- [4] S. M. Sze, *Physics of Semiconductor Devices*, 2nd ed. New York: Wiley, 1981.

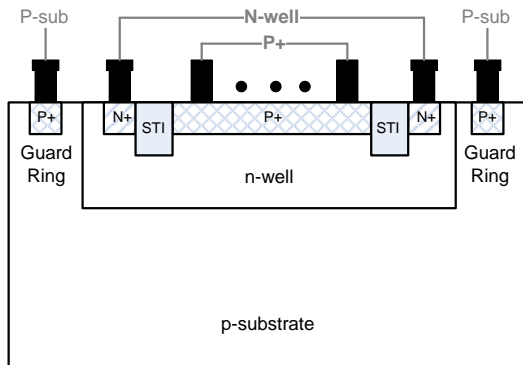


Fig. 1. Schematic cross-section.

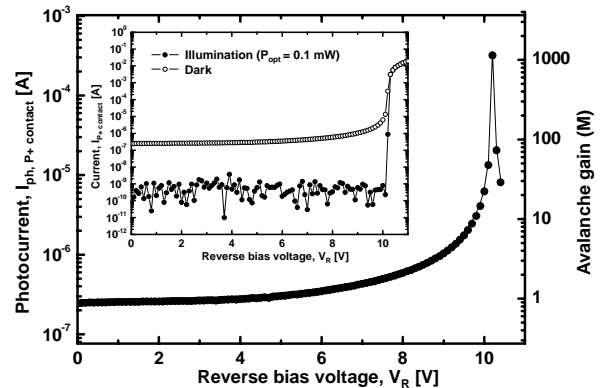


Fig. 2. Photocurrent and avalanche gain of the CMOS-APD. The inset is I-V characteristics.

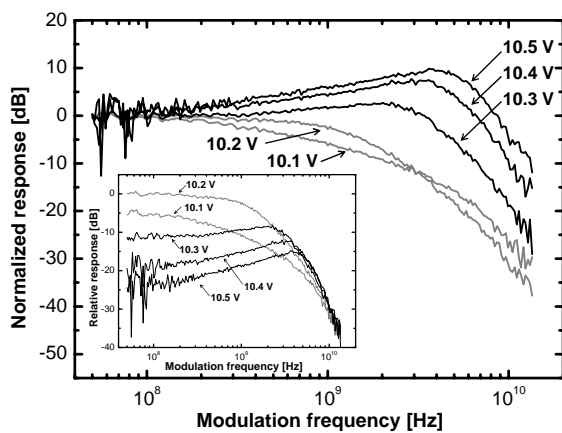


Fig. 3. Normalized photodetection frequency response. The inset shows relative photodetection frequency response. $P_{opt} = 0.2$ mW.

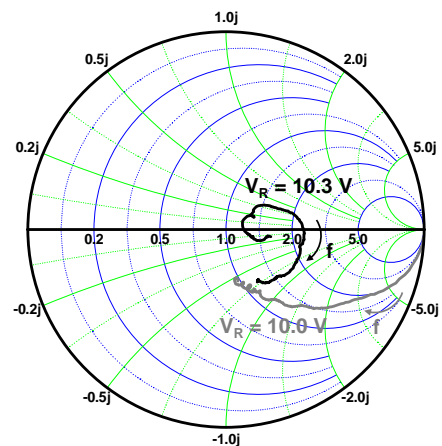


Fig. 4. Reflection coefficient at V_R of 10.0 and 10.3 V. S-parameter is measured from 50 MHz to 13.5 GHz.